Int J Thermophys (2015) 36:2259–2272
DOI 10.1007/s10765-015-1850-2

Thermal Diffusivity and Thermal Conductivity of Five Different Steel Alloys in the Solid and Liquid Phases

B. Wilthan · W. Schützenhöfer · G. Pottlacher

Received: 8 August 2013 / Accepted: 3 February 2015 / Published online: 18 February 2015

Abstract The need for characterization of thermophysical properties of steel and nickel-based alloys was addressed in the FFG-Bridge Project 810999 in cooperation with a partner from industry, Böhler Edelstahl GmbH & Co KG. To optimize numerical simulations of production processes, such as remelting or plastic deformation, additional, and more accurate data were necessary for the alloys under investigation. With a fast ohmic pulse heating circuit system, the temperature-dependent specific electrical resistivity, density, and specific heat capacity for a set of five high alloyed steels were measured. Hence, using the Wiedemann–Franz law with a Lorenz number of $L = 2.45 \times 10^{-8}\,\mathrm{V^2{\cdot}K^{-2}}$, the thermal diffusivity and thermal conductivity could be calculated for the solid and liquid phases up to temperatures of 2500 K. This experimental approach is limited by the following requirements for the specimens: they have to be electrically conducting, the melting point has to be high enough for the implemented pyrometric temperature measurement, and one has to be able to draw wires of the material. The latter restriction is technologically challenging with some of the materials being very brittle. For all samples, electrical and temperature signals are recorded and a fast shadowgraph method is used to measure the volume expansion. For each material under investigation, a set of data including the chemical composition, the density at room temperature, solidus and liquidus temperatures, and the change of enthalpy, resistivity, density, thermal conductivity, and thermal diffusivity as a function of temperature is reported.

B. Wilthan · G. Pottlacher (✉)
Institute of Experimental Physics, Graz University of Technology,
Petersgasse 16, 8010 Graz, Austria
e-mail: Pottlacher@tugraz.at

W. Schützenhöfer
Böhler Edelstahl GmbH & Co KG, Mariazellerstrasse 25, 8605 Kapfenberg, Austria

Keywords 1.3343 · 1.4534 · 1.4944 · 1.6354 · S29225 · Electrical resistivity · Liquid phase · Solid phase · Steel · Steel alloys · Thermal conductivity · Thermal diffusivity

1 Introduction

Numerical simulation of fluid flow, heat transfer, solidification, thermal induced stresses, as well as remelting or plastic deformation, has gained a tremendous significance in steel-working industry branches. With the advent of adequate computing power, full three-dimensional calculation of the determining physical equations has become possible. A major drawback of these simulation techniques is the lack of accurate thermophysical properties. By means of a fast pulse heating technique [1], thermophysical data for the solid and liquid material required for the simulations can be measured. Important input parameters for the heat transfer equation are heat capacity, heat of fusion, density, and thermal conductivity. Since direct measurements of the thermal conductivity of alloys in the liquid state are almost impossible, its estimation from the electrical conductivity using the Wiedemann–Franz law is very useful.

From the huge number of different materials, representative alloys are chosen for this work, e.g., N709 and V720 (a maraging high-strength steel from materials for aviation), P558 from materials for special physical and medical applications, S600 from high-speed steels, and T200 from creep-resistant steels. Some applications [2–6] for these five steel alloys are listed in Table 1. The composition, T_{sol}, T_{liq}, and the density at RT for the five steel alloys are presented in Table 2.

2 Experimental Apparatus and Procedures

2.1 Experimental

To obtain the density at room temperature (RT), our machine department formed cylinders with 50 mm diameter and 50 mm height for each material, which then were weighed in air on a Mettler Toledo PMG 800 Delta apparatus range (0.01 g division). The samples for pulse heating were wire shaped, approximately 0.5 mm in diameter and 70 mm in length. Then these were resistively volume heated as part of a fast capacitor discharge circuit in a N_2 atmosphere and at ambient pressure. In time-resolved measurements with sub-ms resolution, the current through the specimen was measured with a Pearson probe, and the voltage across the specimen was determined with knife-edge contacts and subsequent voltage dividers. The radiance temperatures of the samples were detected with an optical pyrometer operating at 1570 nm, and volume expansions of the samples were measured with a fast acting CCD camera. All the recorded data allowed the calculation of the specific heat and dependencies between the enthalpy, electrical resistivity, temperature, and density of the alloy up into the liquid phase (see Sect. 2.3). In addition to the solidus temperature T_{sol}, the liquidus temperature T_{liq} and the density at RT and results for the thermal conductivity and thermal diffusivity for the solid and liquid phases of all samples are reported as polynomial fits. For more experimental details, see e.g., [7–12].

Table 1 Application of the five steel alloys

Material	Application
N709	Components in the aerospace industry, e.g., high strength screws, bolts, and landing gear components
P558	Surgical implants
S600	Taps, twist drills, reamers, broaching tools, metals saws, milling tools of all types, woodworking tools, cold work tools
T200	Highly stressed components in gas turbines, engines, and rockets, such as turbine blades and disks, shafts, pins, bolts, screws, springs, exhaust reheaters, housing components, thrust nozzles, liners for containers for tubes and rod extruding of copper and copper alloys
V720	Highly stressed components for the aircraft and rocket industries. Constructional and tool steel for hot and cold working tools used for long-time service. Machine tools, pressure vessels, gearwheels, screws, precision parts, tools for hydrostatic presses, cold extrusion tools, cold heading and embossing tools, plastic molds, die casting tools for aluminum and zinc alloys, hot pressing tools, cold pilger mandrels

Table 2 Chemical composition, density, and melting temperatures of the measured alloys

Name	Composition	DIN/EN UNS	Composition (wt%)	T_{sol}	T_{liq}	Density at RT ($kg \cdot m^{-3}$)
N709	X3CrNiMoAl13-8-2	1.4534 S13800	bal. Fe; 12.7 % Cr; 8.2 % Ni; 2.2 % Mo; 1.1 % Al; 0.8 % Si; 0.03 % C	1463 °C 1736 K	1541 °C 1814 K	7727 ± 7
P558		– S29225	bal. Fe; 17.3 % Cr; 10.5 % Mn; 3.3 % Mo; 0.5 % N; 0.45 % Si; 0.2 % C, max. 0.05 % Ni	1375 °C 1648 K	1450 °C 1723 K	7715 ± 6
S600	HS 6-5-2	1.3343 ~ T11302	bal. Fe; 6.4 % W; 5 % Mo; 4.1 % Cr; 1.8 % V; 0.9 % C, 0.3 % Mn; 0.25 % Si	1240 °C 1513 K	1415 °C 1688 K	8099 ± 7
T200	X4NiCrTi25-15	1.4944 S66286	bal. Fe; 25.3 % Ni; 15 % Cr; 2.1 % Ti; 1.5 % Mn; 1.3 % Mo; 0.3 % V; 0.25 % Al; 0.25 % Si; 0.05 % C	1356 °C 1629 K	1446 °C 1719 K	7968 ± 7
V720	X2NiCoMo18-9-5	1.6354 K93120	bal. Fe; 18.5 % Ni; 9.0 % Co; 5.0 % Mo; 0.70 Ti; 0.10 Al; max. 0.10 Si; max. 0.03 C	1365 °C 1638 K	1465 °C 1738 K	8056 ± 8

2.2 Data Reduction Procedure

The surface radiance (J) was determined with a high-speed pyrometer operating at 1570 nm, selected by an interference filter with a bandwidth of 84 nm. To calculate the temperature T of the sample according to Planck's radiation law (Eq. 1), the melting plateau was used as a calibration point. The measured melting temperatures of alloy samples often show a slightly rising temperature during the melting phase, instead of

a totally flat melting plateau. With this setup, the most reliable point is the midpoint of the melting range, i.e., $T_{\mathrm{m}} = \frac{T_{\mathrm{sol}} + T_{\mathrm{liq}}}{2}$ (as listed in Table 2).

$$T = \frac{c_2}{\lambda \cdot \ln\left\{\frac{J_{\mathrm{m}}(T_{\mathrm{m}})}{J(T)} \cdot \left[\mathrm{e}^{\frac{c_2}{\lambda \cdot T_{\mathrm{m}}}} - 1\right] + 1\right\}}, \tag{1}$$

where c_2 is the second radiation constant, λ is the pyrometer center wavelength, and J is the radiance intensity. Here the index m means melting.

The diameter of the specimen at RT is measured using a laser micrometer (Keyence LS-7001 apparatus). During the experiment, the volume expansion of the wire was recorded with a fast CCD camera, which took pictures of the diameter of the specimen about every 5 μs, depending on the preset exposure time. Measured data of voltage, current, and surface radiance were recorded by a fast digital data acquisition system.

Data for thermophysical quantities as a function of time are calculated using Eqs. 2–7. The specific enthalpy H as a function of time t was derived from

$$H(t) = \frac{1}{m} \int_0^t I(t)\, U(t)\, \mathrm{d}t, \tag{2}$$

where m being the mass of the sample, I is the current, and U is the voltage drop across the active length, l, previously measured as the distance between the two knife-edge probes. The electrical resistivity corresponding to the initial geometry at room temperature, ρ_{IG}, is calculated by

$$\rho_{\mathrm{IG}}(t) = \frac{U(t)\, \pi\, r_0^2}{I(t)\, l}, \tag{3}$$

where r_0 denotes the sample radius at room temperature. Due to thermal volume expansion, the sample radius increases during the heating process which led to actual electrical resistivity values computed from

$$\rho(T)_{\mathrm{corr}} = \rho_{\mathrm{IG}}(T)\, \frac{D(T)^2}{D_0^2}, \tag{4}$$

where D_0 and $D(T)$ are the diameter at room temperature and an elevated temperature, respectively. The change of density versus temperature was obtained according to the following equation taking into account the sample expansion $D(T)$ during the heating; $d(T)$ is the actual density at high temperature and d_0 is the density at RT:

$$d(T) = d_{\mathrm{o}}\, \frac{D_0^2}{D(T)^2}. \tag{5}$$

The thermal conductivity λ was calculated from the temperature-dependent electrical resistivity $\rho(T)$ with the Wiedemann–Franz law,

Table 3 List of polynomial fits for N709

Quantity	Units	Polynomial coefficients $y = a + bT + cT^2$			Range T (K)	State
y		a	b	c		
$d(T)$	$\mathrm{kg{\cdot}m^{-3}}$	7.8014×10^3	-0.1179	-1.456×10^{-4}	$1100 < T < 1736$	s
$d(T)$	$\mathrm{kg{\cdot}m^{-3}}$	8.5604×10^3	-1.0464	7.62×10^{-5}	$1814 < T < 2600$	l
$\rho(T)_{\mathrm{IG}}$	$\mu\Omega{\cdot}\mathrm{m}$	1.016	2.74×10^{-4}	6.6×10^{-8}	$1100 < T < 1736$	s
$\rho(T)_{\mathrm{IG}}$	$\mu\Omega{\cdot}\mathrm{m}$	1.394	-8.2×10^{-5}	2.1×10^{-8}	$1814 < T < 2450$	l
$\rho(T)_{\mathrm{corr}}$	$\mu\Omega{\cdot}\mathrm{m}$	1.069	1.90×10^{-4}		$1100 < T < 1736$	s
$\rho(T)_{\mathrm{corr}}$	$\mu\Omega{\cdot}\mathrm{m}$	1.152	1.74×10^{-4}		$1814 < T < 2450$	l
$H(T)$	$\mathrm{kJ{\cdot}kg^{-1}}$	-2.329×10^2	0.6627		$1100 < T < 1736$	s
$H(T)$	$\mathrm{kJ{\cdot}kg^{-1}}$	-2.746×10^2	0.8254		$1814 < T < 2550$	l
$\lambda(T)$	$\mathrm{W{\cdot}m^{-1}{\cdot}K^{-1}}$	4.98	1.474×10^{-2}		$1100 < T < 1736$	s
$\lambda(T)$	$\mathrm{W{\cdot}m^{-1}{\cdot}K^{-1}}$	8.28	1.217×10^{-2}		$1814 < T < 2450$	l
$a(T)$	$\mathrm{m^2{\cdot}s^{-1}}$	5.03×10^{-7}	3.41×10^{-9}		$1100 < T < 1736$	s
$a(T)$	$\mathrm{m^2{\cdot}s^{-1}}$	8.76×10^{-8}	2.88×10^{-9}		$1814 < T < 2450$	l

"s" means solid state; "l" designates liquid state

$$\lambda(T) = \frac{LT}{\rho(T)}. \tag{6}$$

In this work, the theoretical value for the Lorentz number $L (L = 2.45 \times 10^{-8}\ \mathrm{V^2{\cdot}K^{-2}})$ is used, assuming that it is invariant within the region of interest [13]. The thermal diffusivity a is then estimated from the thermal conductivity, specific heat capacity at constant pressure c_p, and temperature-dependent density $d(T)$, as

$$a = \frac{\lambda}{c_p d} \equiv \frac{LT}{\rho_{\mathrm{IG}} c_p d_0}. \tag{7}$$

From the right-hand side of Eq. 7, it can be seen that the thermal diffusivity is not dependent on the volume expansion under the assumption of the constant Lorentz ratio within the measuring temperature range.

The only data required for the calculation, electrical data, and temperature can be measured with a relatively low uncertainty [14]. Assuming the same principle, several papers have already been published from our work group dealing with steel or Ni-based alloys, presenting also the change of enthalpy, resistivity, density, thermal conductivity, and thermal diffusivity as a function of temperature [9–11,15–19].

2.3 Results for Density, Electrical Resistivity, Specific Enthalpy, Thermal Conductivity, and Thermal Diffusivity

Due to the number of equations necessary to present all results for each material in a usable format, polynomial fits are given in Tables 3, 4, 5, 6, 7 and 8. The values at the

Table 4 List of polynomial fits for P558

Quantity	Units	Polynomial coefficients $y = a + bT + cT^2 + dT^3$				Range T (K)	State
y		a	b	c	d		
$d(T)$	$kg{\cdot}m^{-3}$	7.7185×10^3	0.0525	-2.222×10^{-4}		$1000 < T < 1648$	s
$d(T)$	$kg{\cdot}m^{-3}$	8.5116×10^3	−0.9365	6.46×10^{-5}		$1723 < T < 2500$	l
$\rho(T)_{IG}$	$\mu\Omega{\cdot}m$	0.1076	1.92×10^{-3}	-1.112×10^{-6}	2.278×10^{-10}	$1200 < T < 1648$	s
$\rho(T)_{IG}$	$\mu\Omega{\cdot}m$	1.344	-5.65×10^{-5}	1.49×10^{-8}		$1723 < T < 2500$	l
$\rho(T)_{corr}$	$\mu\Omega{\cdot}m$	0.785	4.77×10^{-4}	-7.8×10^{-8}		$1200 < T < 1648$	s
$\rho(T)_{corr}$	$\mu\Omega{\cdot}m$	1.224	7.58×10^{-5}	1.75×10^{-8}		$1723 < T < 2500$	l
$H(T)$	$kJ{\cdot}kg^{-1}$	-3.127×10^2	0.6871			$1200 < T < 1648$	s
$H(T)$	$kJ{\cdot}kg^{-1}$	-3.393×10^2	0.8505			$1723 < T < 2500$	l
$\lambda(T)$	$W{\cdot}m^{-1}{\cdot}K^{-1}$	7.40	1.354×10^{-2}			$1200 < T < 1648$	s
$\lambda(T)$	$W{\cdot}m^{-1}{\cdot}K^{-1}$	7.40	1.321×10^{-2}			$1723 < T < 2500$	l
$a(T)$	$m^2{\cdot}s^{-1}$	8.59×10^{-7}	3.12×10^{-9}			$1200 < T < 1648$	s
$a(T)$	$m^2{\cdot}s^{-1}$	5.99×10^{-8}	2.86×10^{-9}			$1723 < T < 2500$	l

"s" means solid state; "l" designates liquid state

Table 5 List of polynomial fits for S600

Quantity	Units	Polynomial coefficients $y = a + bT + cT^2$			Range T (K)	State
y		a	b	c		
$d(T)$	$\mathrm{kg{\cdot}m^{-3}}$	8.0846×10^{3}	0.0926	-2.211×10^{-4}	$1050 < T < 1513$	s
$d(T)$	$\mathrm{kg{\cdot}m^{-3}}$	9.1555×10^{3}	−1.3429	1.161×10^{-4}	$1688 < T < 2100$	l
$\rho(T)_{\mathrm{IG}}$	μΩ·m	0.5747	8.407×10^{-4}	-2.479×10^{-7}	$1100 < T < 1513$	s
$\rho(T)_{\mathrm{IG}}$	μΩ·m	1.2860	1.57×10^{-5}		$1688 < T < 2100$	l
$\rho(T)_{\mathrm{corr}}$	μΩ·m	0.576	8.19×10^{-4}	-2.07×10^{-7}	$1100 < T < 1513$	s
$\rho(T)_{\mathrm{corr}}$	μΩ·m	1.113	2.13×10^{-4}		$1688 < T < 2100$	l
$H(T)$	$\mathrm{kJ{\cdot}kg^{-1}}$	3.532×10^{2}	−0.2618	4.121×10^{-4}	$1100 < T < 1513$	s
$H(T)$	$\mathrm{kJ{\cdot}kg^{-1}}$	-6.209×10^{2}	1.1514		$1688 < T < 2400$	l
$\lambda(T)$	$\mathrm{W{\cdot}m^{-1}{\cdot}K^{-1}}$	6.90	1.369×10^{-2}		$1100 < T < 1513$	s
$\lambda(T)$	$\mathrm{W{\cdot}m^{-1}{\cdot}K^{-1}}$	8.13	1.185×10^{-2}		$1688 < T < 2100$	l
$a(T)$	$\mathrm{m^2{\cdot}s^{-1}}$	8.56×10^{-8}	1.95×10^{-9}		$1688 < T < 2100$	l

"s" means solid state; "l" designates liquid state

Table 6 List of polynomial fits for T200

Quantity	Units	Polynomial coefficients $y = a + bT + cT^2$			Range T (K)	State
y		a	b	c		
$d(T)$	$\mathrm{kg{\cdot}m^{-3}}$	8.0913×10^{3}	−0.3362	-9.30×10^{-5}	$1100 < T < 1629$	s
$d(T)$	$\mathrm{kg{\cdot}m^{-3}}$	7.8426×10^{3}	−0.5937	3.15×10^{-5}	$1719 < T < 2500$	l
$\rho(T)_{\mathrm{IG}}$	μΩ·m	1.1426	9.41×10^{-5}		$1200 < T < 1629$	s
$\rho(T)_{\mathrm{IG}}$	μΩ·m	1.2962	8.8×10^{-6}		$1719 < T < 2600$	l
$\rho(T)_{\mathrm{corr}}$	μΩ·m	1.0711	2.105×10^{-4}		$1200 < T < 1629$	s
$\rho(T)_{\mathrm{corr}}$	μΩ·m	1.3095	1.171×10^{-4}		$1719 < T < 2500$	l
$H(T)$	$\mathrm{kJ{\cdot}kg^{-1}}$	-3.456×10^{2}	0.7293		$1200 < T < 1629$	s
$H(T)$	$\mathrm{kJ{\cdot}kg^{-1}}$	-5.88×10^{1}	0.7013		$1719 < T < 2600$	l
$\lambda(T)$	$\mathrm{W{\cdot}m^{-1}{\cdot}K^{-1}}$	5.38	1.407×10^{-2}		$1200 < T < 1629$	s
$\lambda(T)$	$\mathrm{W{\cdot}m^{-1}{\cdot}K^{-1}}$	5.37	1.317×10^{-2}		$1719 < T < 2600$	l
$a(T)$	$\mathrm{m^2{\cdot}s^{-1}}$	4.73×10^{-7}	2.97×10^{-9}		$1200 < T < 1629$	s
$a(T)$	$\mathrm{m^2{\cdot}s^{-1}}$	1.04×10^{-7}	3.28×10^{-9}		$1719 < T < 2600$	l

"s" means solid state; "l" designates liquid state

melting transition are presented separately in Table 9. All given data for the specific heat capacity are derived from the slope of the linear fit of the specific heat capacity. Thus, in the solid phase, values only have been considered to 100 K below the solidus temperature.

Table 7 List of polynomial fits for V720

Quantity	Units	Polynomial coefficients $y = a + bT + cT^2$			Range T (K)	State
y		a	b	c		
$d(T)$	$\mathrm{kg{\cdot}m^{-3}}$	8.0395×10^3	0.127	-2.35×10^{-4}	$1200 < T < 1638$	s
$d(T)$	$\mathrm{kg{\cdot}m^{-3}}$	8.9429×10^3	−1.056	7.17×10^{-5}	$1738 < T < 3300$	l
$\rho(T)_{\mathrm{IG}}$	$\mu\Omega{\cdot}$m	0.989	1.58×10^{-4}		$1150 < T < 1638$	s
$\rho(T)_{\mathrm{IG}}$	$\mu\Omega{\cdot}$m	1.228	4.6×10^{-5}	-6.4×10^{-9}	$1738 < T < 2950$	l
$\rho(T)_{\mathrm{corr}}$	$\mu\Omega{\cdot}$m	0.909	2.49×10^{-4}		$1150 < T < 1638$	s
$\rho(T)_{\mathrm{corr}}$	$\mu\Omega{\cdot}$m	1.109	1.77×10^{-4}		$1738 < T < 2950$	l
$H(T)$	$\mathrm{kJ{\cdot}kg^{-1}}$	4.253×10^2	−0.305	3.353×10^{-4}	$1100 < T < 1638$	s
$H(T)$	$\mathrm{kJ{\cdot}kg^{-1}}$	-2.20×10^2	0.7852		$1738 < T < 3100$	l
$\lambda(T)$	$\mathrm{W{\cdot}m^{-1}{\cdot}K^{-1}}$	5.15	1.655×10^{-2}		$1200 < T < 1638$	s
$\lambda(T)$	$\mathrm{W{\cdot}m^{-1}{\cdot}K^{-1}}$	1.18	1.835×10^{-2}		$1738 < T < 2950$	l
$a(T)$	$\mathrm{m^2{\cdot}s^{-1}}$	1.87×10^{-7}	2.90×10^{-9}		$1738 < T < 2950$	l

"s" means solid state; "l" designates liquid state

Table 8 Values of resistivity and enthalpy at solidus and liquidus, and specific heat capacity for the end of the solid and liquid phases

Alloy	$\rho_{\mathrm{IG,sol}}$ ($\mu\Omega{\cdot}$m)	$\rho_{\mathrm{IG,liq}}$ ($\mu\Omega{\cdot}$m)	$\rho_{\mathrm{corr,sol}}$ ($\mu\Omega{\cdot}$m)	$\rho_{\mathrm{corr,liq}}$ ($\mu\Omega{\cdot}$m)	H_{sol} ($\mathrm{kJ{\cdot}kg^{-1}}$)	H_{liq} ($\mathrm{kJ{\cdot}kg^{-1}}$)	ΔH ($\mathrm{kJ{\cdot}kg^{-1}}$)	$c_{p,\mathrm{sol}}$ ($\mathrm{J{\cdot}kg^{-1}{\cdot}K^{-1}}$)	$c_{p,\mathrm{liq}}$ ($\mathrm{J{\cdot}kg^{-1}{\cdot}K^{-1}}$)
N709	1.29	1.31	1.40	1.47	918	1223	305	663	825
P558	1.27	1.29	1.36	1.41	820	1126	306	687	851
S600	1.28	1.31	1.28	1.47	901	1323	422	–	1151
T200	1.30	1.31	1.30	1.31	842	1147	304	729	701
V720	1.25	1.29	1.32	1.42	825	1145	320	–	785

Table 9 Relative expanded uncertainties ($k = 2$) for specific enthalpy as a function of temperature, solid phase H_{s}, liquid phase H_{l}, electrical resistivity (ρ) with initial geometry as a function of temperature, heat capacity (c_p) in solid and liquid phases, and thermal diffusivity (a) in solid and liquid phases

Alloy	$U(H_{\mathrm{s}})$ (%)	$U(H_{\mathrm{l}})$ (%)	$U(\rho)$ (%)	$U(c_{p,\mathrm{sol}})$ (%)	$U(c_{p,\mathrm{liq}})$ (%)	$U(a_{\mathrm{sol}})$ (%)	$U(a_{\mathrm{liq}})$ (%)
L306	± 5	± 4	± 2	± 6	± 4	± 8	± 6
N709	± 6	± 3.8	± 1.9	± 4.2	± 3.3	± 5.8	± 4.9
P558	± 5.5	± 3.6	± 2.2	± 6.6	± 2.4	± 8.4	± 4.3
S600	± 5.5	± 4.0	± 1.8	–	± 2.1	–	± 3.9
T200	± 6	± 3.5	± 2.0	± 7.2	± 3.5	± 8.9	± 3.5
V720	± 16 − 12	± 4.5	± 3.2	–	± 14	–	± 6.5

3 Discussion

The results for four investigated alloys show a similar behavior of $H(T)$ in both the liquid and solid phases, as shown in Fig. 1. Only S600 stands out, and its specific enthalpy is 20 % to 30 % higher at a comparable temperature. From the slope of these results, we obtain c_p values for both phases. In the liquid phase, c_p is a constant value by theory (see, for example, Grimvall [20]), whereas c_p in the solid phase typically varies with temperature. When a linear fit to our measured values can describe the specific enthalpy in the solid phase, we estimate c_p also there, but the validity strongly depends on structural and phase changes in the solid material. To be cautious, c_p values given for the solid phase are only valid in a range of 100 K below the solidus temperature. No c_p values are given in Table 8 for S600 and V720 before melting where the enthalpy can only be fitted with a quadratic polynomial, as c_p is only described by the slope of a linear polynomial.

Resistivities at the initial geometry (see Fig. 2) lie within two bands, separated by up to 3 %; an upper band with N709, S600, and T200 and a lower one with P558 and V720. In the solid phase, the resistivity of all materials increases with temperature. The transition from solidus to liquidus is accompanied by a sudden increase in resistivity, and in the first 500 K to 1300 K into the liquid phase, the $\rho(T)$ values show a small increase or can almost be assumed as constant considering the stated uncertainties.

Using the values of c_p from Table 8 and the temperature-dependent resistivity data at the initial geometry, the thermal diffusivity is calculated from Eq. 7 and curves for all materials are plotted in Fig. 3. Each steel alloy shows an increase in thermal

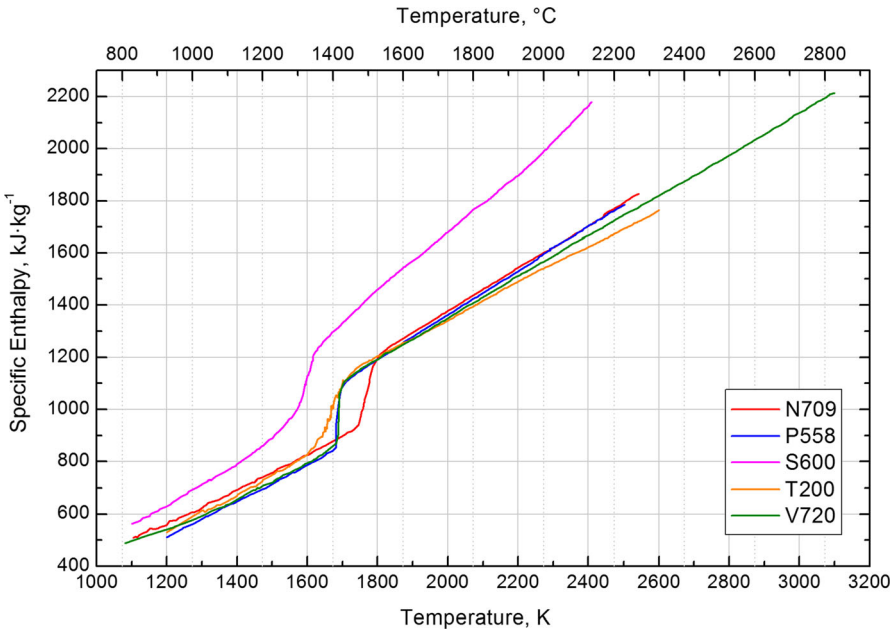

Fig. 1 Enthalpy as a function of temperature for five alloys

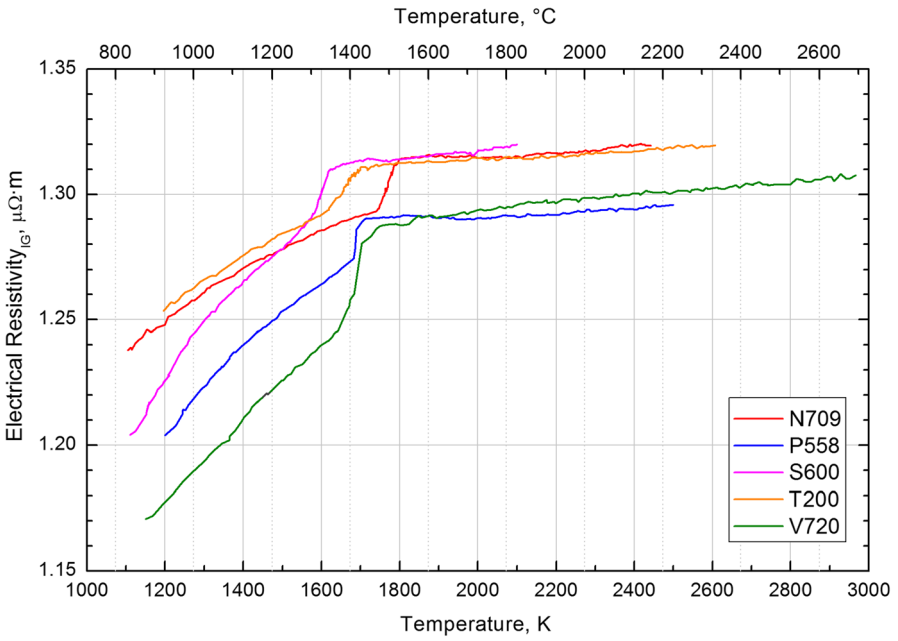

Fig. 2 Resistivity with initial geometry as a function of temperature for five alloys

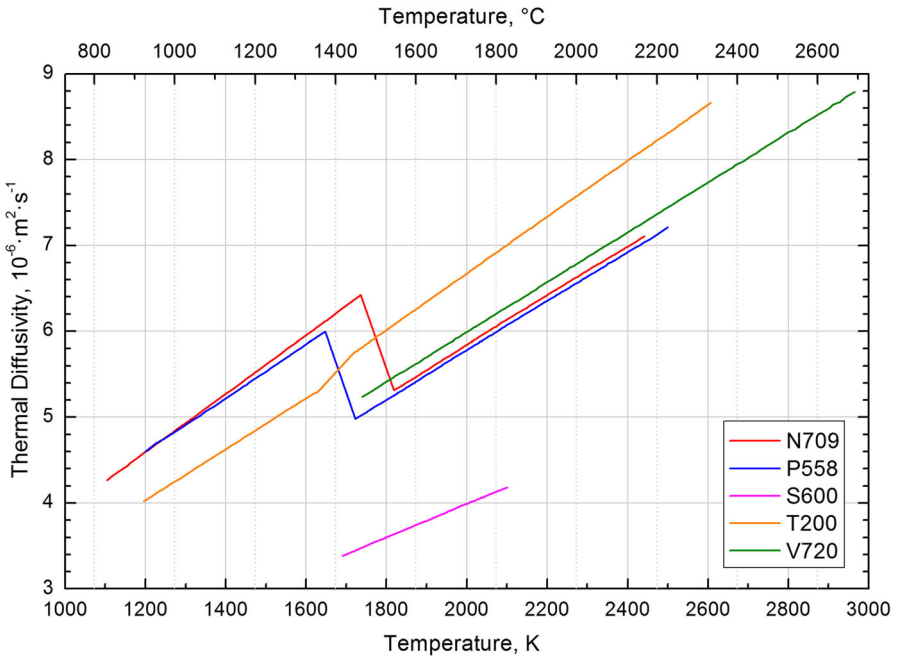

Fig. 3 Thermal diffusivity as a function of temperature for five alloys

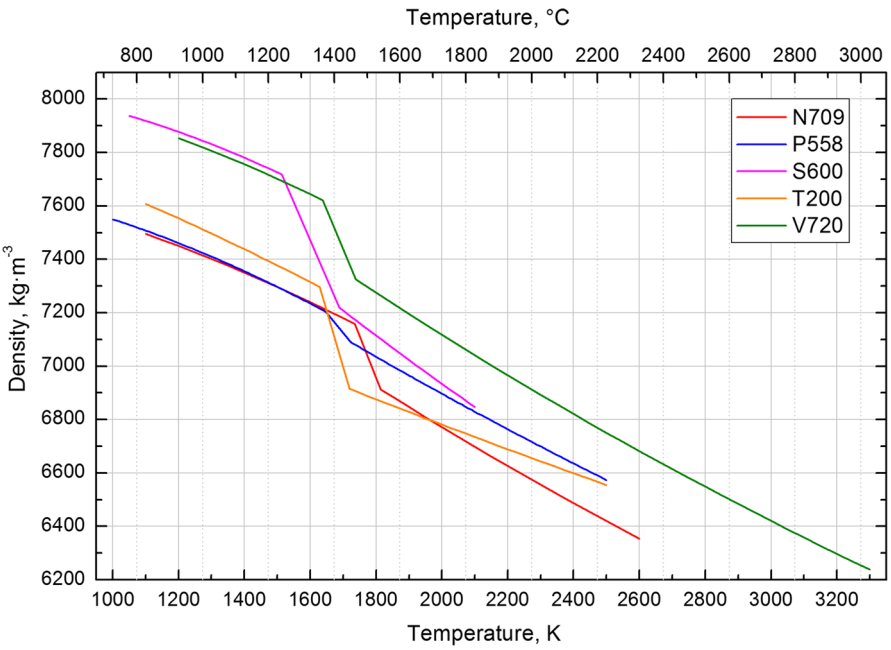

Fig. 4 Density as a function of temperature for five alloys

diffusivity with temperature in both phases. Above melting, S600 has the lowest and T200 the highest values of a. Only for the material T200, the values increase at the transition from solidus to liquidus whereas for N709 and P558 a significant decrease is observed at this transition. With no c_p results for S600 and V720 in the solid phase, only values in the liquid phase are calculated for these alloys. However, the reader could estimate c_p for both materials using the first derivative of the polynomial fits of $H(T)$.

Figure 4 depicts density values as a function of temperature. For all the materials, the density is decreasing with temperature. The highest values are recorded for S600, V720, and T200, while the densities of P558 and N709 are about 350 kg·m^{-3} lower. From RT up to T_{sol} (T_{liq}), a decrease of density is observed. The highest decrease at the melting point represents those of S600: 4.69 % (14.9 %) and T200: 8.42 % (13.2 %). A minimal decrease of density at melting is observed for P558: 6.66 % (8.1 %), and values for N709 7.37 % (10.5 %) and V720: 5.39 % (9.0 %) are in between. A rule of thumb [21] estimates a 7 % density decrease up to solidus, which is roughly confirmed here.

Data obtained from the expansion measurements with a fast CCD camera were applied for the correction of electrical resistivity values. Figure 5 shows corrected values of the electrical resistivity as a function of temperature. In the liquid phase, steeper increase rates of ρ_{corr} are observed for all specimens; however, the order between the data, lowest to highest value, is not changed by including this correction.

Figure 6 depicts the thermal conductivity as a function of temperature, as calculated with the Wiedemann–Franz law (Eq. 6). Due to its density versus temperature

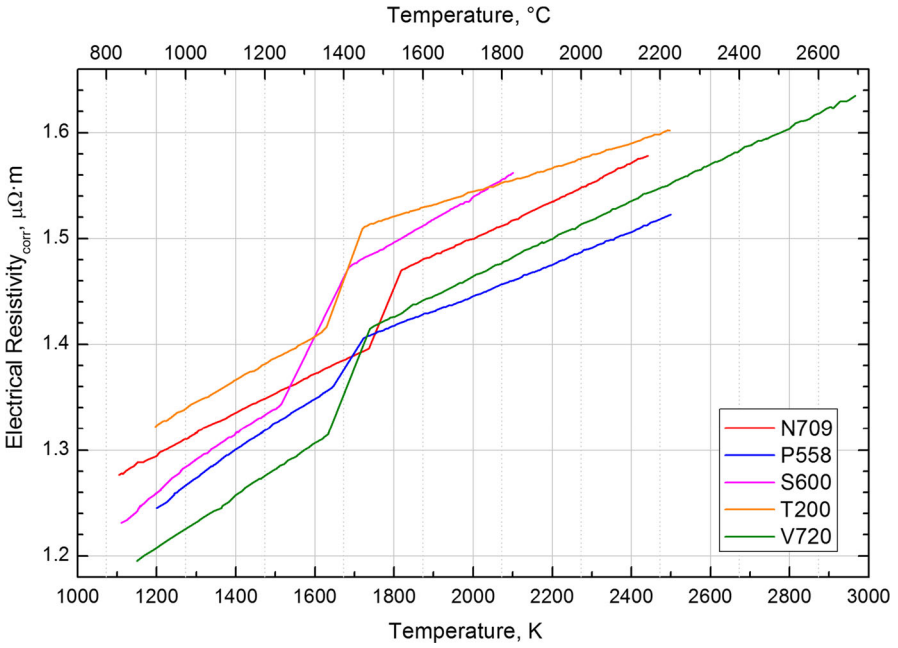

Fig. 5 Resistivity as a function of temperature for five alloys

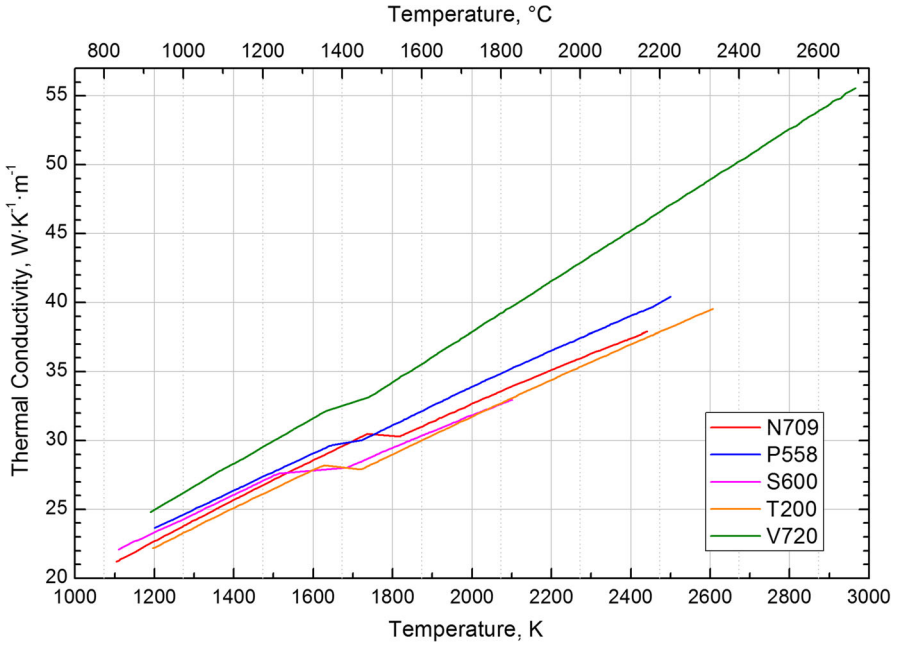

Fig. 6 Thermal conductivity as a function of temperature for five alloys

dependence, the results for V720 are significantly higher than those for the other four materials. Regarding the thermal conductivity of metals and alloys in the solid state, it has to be noted that it is important to include both electronic and lattice components, as shown in the theoretical work of Klemens [13]. The measurement principle used in this work can only measure electronic components, but for Fe-Cr-Ni alloys, Klemens suggests lattice contributions that vary from 4.8 $W \cdot m^{-1} \cdot K^{-1}$ for Nimonic 80 and Inconel 718 [13] up to values of 6.8 $W \cdot m^{-1} \cdot K^{-1}$ for SRM 735 and 7.4 $W \cdot m^{-1} \cdot K^{-1}$ for Nimonic 75. These influences were discussed in our previous work for Inconel 718 [7] and after including a correction for the lattice parameter, the experimental values were in good agreement with existing literature values for that alloy. From that reason, for the solid state, a value of about 5 $W \cdot m^{-1} \cdot K^{-1}$ to 6 $W \cdot m^{-1} \cdot K^{-1}$ should be added to the thermal conductivity values reported here. In the liquid phase, no such compensation is necessary, as there is no additional influence from the lattice contribution to the thermal conductivity.

3.1 Uncertainties

All uncertainties reported in Table 9 represent expanded relative uncertainties with a coverage factor of $k = 2$ (95 %), calculated following the GUM for all specimens [22]. Corresponding uncertainty bars are not depicted in the individual figures.

Acknowledgments This research was supported by Böhler Edelstahl GmbH & Co KG and the "Forschungsförderungsgesellschaft mbH, Sensengasse 1, 1090 Wien, Austria," by Project 810999.

References

1. G. Pottlacher, K. Aziz, A. Schmon, High Temp. High Press. **43**, 377 (2012)
2. Werbebroschüre N709, Böhler Edelstahl (2015), http://www.bohler.de/german/files/N709DE.pdf. Accessed 14 Jan 2015
3. Werbebroschüre P558, Böhler Edelstahl (2015), http://www.bohler.at/deutsch/files/downloads/P558_Info_D.pdf. Accessed 14 Jan 2015
4. Werbebroschüre S600, Böhler Edelstahl (2015), http://www.bohler-edelstahl.com/files/S600DE.pdf. Accessed 14 Jan 2015
5. Werbebroschüre T200, Böhler Edelstahl (2015), http://www.bohler-international.com/english/files/BW100DE_Luftfahrt.pdf. Accessed 14 Jan 2015
6. Werbebroschüre V720, Böhler Edelstahl (2015), http://www.bohler.de/german/files/V720DE.pdf. Accessed 14 Jan 2015
7. G. Pottlacher, H. Hosaeus, A. Seifter, E. Kaschnitz, Scand. J. Metall. **31**, 161 (2002)
8. B. Wilthan, R. Tanzer, W. Schützenhöfer, G. Pottlacher, Rare Met. **25**, 529 (2006)
9. B. Wilthan, K. Preis, R. Tanzer, W. Schützenhöfer, G. Pottlacher, J. Alloys Compd. **452**, 102 (2007)
10. B. Wilthan, K. Preis, R. Tanzer, W. Schützenhöfer, G. Pottlacher, Thermochim. Acta **465**, 83 (2007)
11. B. Wilthan, G. Pottlacher, High Temp. High Press. **40**, 301 (2011)
12. S. Mehmood, U. Klotz, G. Pottlacher, Metall. Mater. Trans. A **43**, 5029 (2012). doi:10.1007/s11661-012-1319-x
13. P.G. Klemens, R.K. Williams, Int. Met. Rev. **31**, 197 (1986)
14. B. Wilthan, H. Reschab, R. Tanzer, W. Schützenhöfer, G. Pottlacher, Int. J. Thermophys. **29**, 434 (2008)
15. A. Seifter, K. Boboridis, V. Didoukh, G. Pottlache, H. Jäger, High Temp. High Press. **29**, 411 (1997)
16. A. Seifter, G. Pottlacher, H. Jäger, G. Groboth, E. Kaschnitz, Ber. Bunsen Ges. **102**, 1266 (1998)
17. H. Hosaeus, A. Seifter, E. Kaschnitz, G. Pottlacher, High Temp. High Press. **33**, 405 (2001)

18. S. Rudtsch, H.-P. Ebert, F. Hemberger, G. Barth, R. Brandt, U. Groß, W. Hohenauer, K. Jaenicke-Roessler, E. Kaschnitz, E. Pfaff, W. Pößnecker, G. Pottlacher, M. Rhode, B. Wilthan, Int. J. Thermophys. **26**, 855 (2005)
19. T. Hüpf, C. Cagran, E. Kaschnitz, G. Pottlacher, Thermochim. Acta **494**, 40 (2009)
20. G. Grimvall, in *Thermophysical Properties of Materials: Enlarged and Revised Edition* (North-Holland, Amsterdam, 1999), ISBN-10:0444544232, ISBN-13:978–0444544230
21. F. Richter, Die physikalischen Eigenschaften der Stähle "Das 100 Stähle Programm" http://portal.tugraz.at/portal/page/portal/Files/i5110/files/Forschung/Thermophysik/Staehle-Richter.pdf. Accessed 14 Jan 2015
22. Deutsches Institut für Normung e.V. DIN. Leitfaden zur Angabe der Unsicherheit beim Messen. Beuth Verlag GmbH, 1st edn., 1995; original: Guide to the Expression of Uncertainty in Measurement (ISO, Geneva, 1993)